Dynamic Biodistribution of Extracellular Vesicles *in Vivo* Using a Multimodal Imaging Reporter

Charles P. Lai,[†,∥,*] Osama Mardini,[†] Maria Ericsson,[#] Shilpa Prabhakar,[†] Casey A. Maguire,[†] John W. Chen,[§,⊥] Bakhos A. Tannous,[†,‡,∥,△] and Xandra O. Breakefield[†,‡,∥,△,*]

[†]Department of Neurology, [‡]Department of Radiology, [§]Center for Systems Biology, and [⊥]Center for Molecular Imaging Research, Massachusetts General Hospital, Charlestown, Massachusetts 02129, United States, and [∥]Program in Neuroscience and [#]Conventional Electron Microscopy Core, Harvard Medical School, Boston, Massachusetts 02115, United States. [△]B. A. Tannous and X. O. Breakefield contributed equally to this work.

ABSTRACT Extracellular vesicles (EVs) are nanosized vesicles released by normal and diseased cells as a novel form of intercellular communication and can serve as an effective therapeutic vehicle for genes and drugs. Yet, much remains unknown about the *in vivo* properties of EVs such as tissue distribution, blood levels, and urine clearance, important parameters that will define their therapeutic effectiveness and potential toxicity. Here we combined *Gaussia* luciferase and metabolic biotinylation to create a sensitive EV reporter (EV-GlucB) for multimodal imaging *in vivo*, as well as monitoring of EV levels in the organs and biofluids *ex vivo* after administration of EVs. Bioluminescence and fluorescence-mediated tomography imaging on mice displayed a predominant localization of intravenously administered EVs in the spleen followed by the liver. Monitoring EV signal in the organs, blood, and urine further revealed that the EVs first undergo a rapid distribution phase followed by a longer elimination phase *via* hepatic and renal routes within six hours, which are both faster than previously reported using dye-labeled EVs. Moreover, we demonstrate systemically injected EVs can be delivered to tumor sites within an hour following injection. Altogether, we show the EVs are dynamically processed *in vivo* with accurate spatiotemporal resolution and target a number of normal organs as well as tumors with implications for disease pathology and therapeutic design.

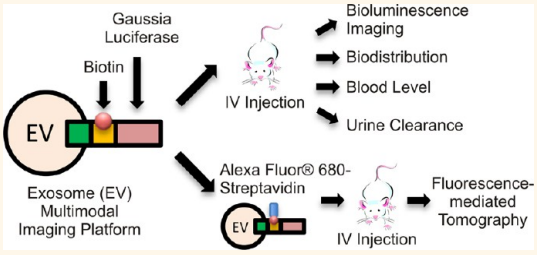

KEYWORDS: exosomes · microvesicles · bioluminescence · fluorescence · biotin · biodistribution · delivery

Exosomes and microvesicles, collectively termed extracellular vesicles (EVs), are nanometer sized (40−1000 nm diameter) particles endogenously released by cells, capable of delivering lipids, proteins, mRNAs, microRNAs (miRNAs), and other noncoding RNAs.[1,2] While specialized physical conduits, such as membrane nanotubes and gap junctions, are spatially limited and require direct cell-to-cell contacts,[3,4] EVs can mediate communication between both neighboring and distant cells, thereby emerging as a novel form of intercellular communication and delivery vehicle. Under pathological conditions such as cancer, tumors produce an abundance of EVs that contain a select subset of cellular proteins, mRNAs, and miRNAs that manipulate normal cells in their microenvironment to enhance angiogenesis, invasiveness, immune suppression, and tumor growth.[5−7] Further, EVs released from melanoma cells are capable of preconditioning sentinel lymph nodes and bone marrow progenitor cells to facilitate metastases of these tumors.[8,9] In addition, recent studies have shown promising results in using EVs as novel therapeutic vehicles in cancer immunotherapy and suicide therapy, as well as delivery of RNA-interference and drugs.[1,2,10−12] Unlike its artificial synthetic counterpart, liposomes, EVs are poorly immunogenic, while still capable of shielding "therapeutic cargoes" from rapid degradation *in vivo*, as well as overcoming biological barriers, such as the blood−brain barrier.[3,4,13−17] However, much remains unexplored about the *in vivo* properties of EVs, including tissue distribution, blood levels, and clearance dynamics, important parameters that will define their therapeutic effectiveness and potential toxicity in clinical applications.

Here we designed a highly sensitive and versatile EV reporter system that enables multimodal *in vivo* imaging, as well as tracking of EV biodistribution and clearance of

* Address correspondence to lai.charles@mgh.harvard.edu; breakefield@hms.harvard.edu.

Received for review September 22, 2013 and accepted December 30, 2013.

Published online January 02, 2014
10.1021/nn404945r

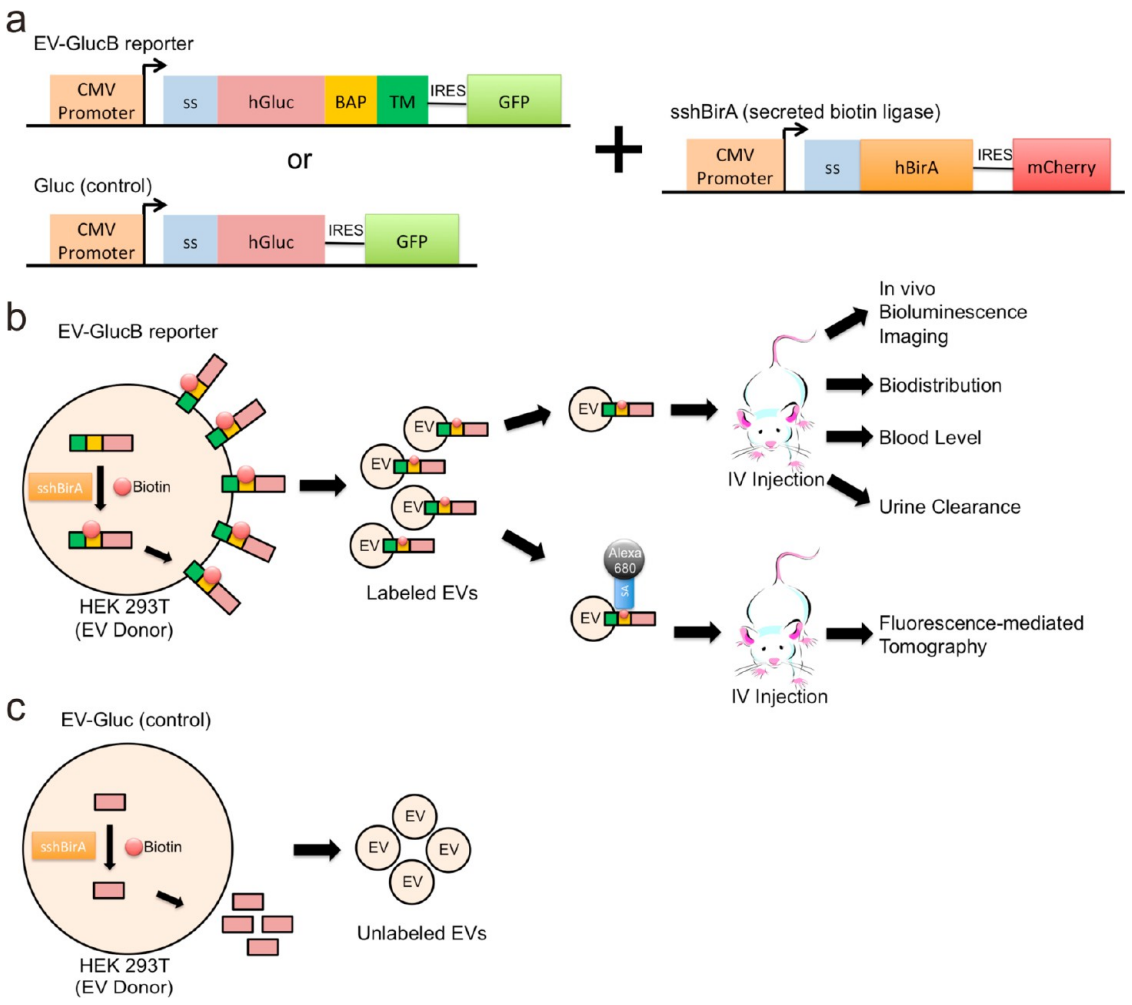

Figure 1. Schematic diagram for *in vivo* multimodal imaging of EVs. (a) Membrane-bound Gluc (GlucB) or Gluc (control) and the secreted form of humanized bacterial biotin ligase (sshBirA) were delivered *via* lentivectors to HEK 293T cells for stable expression. (b) Upon expression and EV production by the cells, the sshBirA tags the BAP sequence of GlucB with a single biotin moiety at a specific lysine residue, which is then displayed on the cell surface,[20] as well as on the EV surface. EVs were isolated from conditioned medium of cells and injected intravenously (iv) *via* tail or retro-orbital veins into nude mice for bioluminescence and fluorescence-mediated tomography (FMT) imaging. For bioluminescence imaging, coelentrazine, a Gluc substrate, was iv-administered immediately prior to imaging. For FMT imaging, isolated EVs were conjugated with streptavidin-Alexa680 prior to administration into nude mice. (c) EVs derived from cells synthesizing naturally secreted Gluc were used as controls, as the Gluc is not present in the EVs. Abbreviations: BAP, biotin acceptor peptide; CMV, cytomegalovirus; GFP, green fluorescent protein; hBirA, humanized biotin ligase; hGluc, humanized *Gaussia* luciferase; IRES, internal ribosome entry site; SA, streptavidin; ss, signal peptide; TM, transmembrane domain of platelet-derived growth factor receptor.

exogenous EVs over time. We engineered EVs to display a membrane reporter, termed EV-GlucB, consisting of Gluc fused to a biotin acceptor domain, which is metabolically biotinylated when expressed in mammalian cells in the presence of biotin ligase. These EVs exhibit a strong bioluminescent signal when incubated with the Gluc substrate coelentrazine (CTZ). In addition, biotin on the surface allows EVs to be conjugated to any labeled streptavidin, which can then be imaged noninvasively *in vivo* using different techniques including fluorescence-mediated tomography (FMT). Furthermore, *ex vivo* analysis of tissues/blood/urine with the Gluc assay allows evaluation of biodistribution and clearance of EVs. Combing this new EV reporter system with noninvasive *in vivo* imaging and *ex vivo* analyses, we examined the fate of systemically injected EVs in mice.

RESULTS AND DISCUSSION

Generation of EV-GlucB. To display both Gluc and biotin on the surface of EVs, we took advantage of our previously published reporter consisting of a fusion between a membrane-bound variant of the Gluc reporter and a biotin acceptor peptide (BAP; GlucB), which exposes both on the surface of cells and vesicles.[5−7,18] Human embryonic kidney (HEK) 293T cells were stably transduced with lentivirus vectors encoding two expression cassettes: (1) GlucB or Gluc (control, with Gluc being a secreted protein) and green fluorescent protein (GFP) separated by an internal

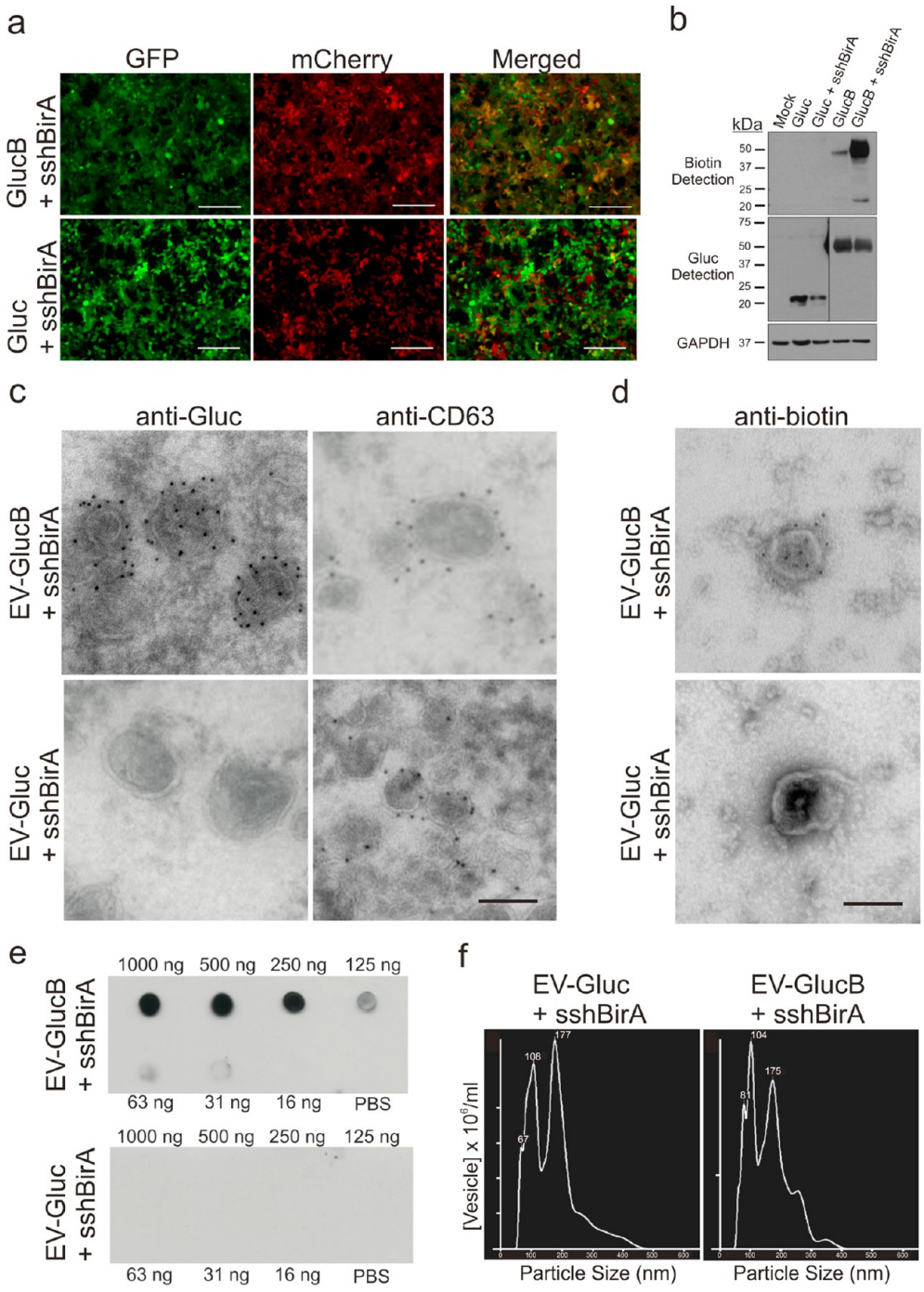

Figure 2. GlucB and sshBirA label and biotinylate EVs on the surface. (a, b) Stable HEK293T cells expressing sshBirA with GlucB or Gluc. (a) Live-cell imaging of HEK293T cells stably transduced with GlucB-IRES-GFP or Gluc-IRES-GFP vectors, both with sshBirA-IRES-mCherry. Bar, 100 μm. (b) Western blot analysis showing enhanced biotinylation of cells stably expressing GlucB with sshBirA, as compared to GlucB alone. No biotinylation was detected in cells expressing Gluc alone or Gluc with sshBirA. Immunoblotting with anti-Gluc antibodies showed Gluc and GlucB at expected sizes (Gluc: 20 kDa; GlucB: 42 kDa). A low level of biotinylated BAP domain (22 kDa) was also detected in GlucB and GlucB ± sshBirA samples. Mock transduced HEK293T were used as a negative control. GAPDH was immunoprobed as a loading control. (c, d) Transmission electron micrograph (TEM) demonstrating biotinylation and Gluc labeling of EV-GlucB on the membrane. (c) Sectioned EVs were immunolabeled with either anti-CD63, an exosome marker,[21] or anti-Gluc antibody followed by gold-conjugated secondary antibody to visualize GlucB labeling of EVs on the membrane, with EV-Gluc showing no Gluc signal but having the CD63 signal. Bar, 100 nm. (d) EVs in suspension were immunolabeled with an antibiotin antibody followed by 10 nm gold-conjugated secondary antibody, and biotinylation of EV-GlucB but not EV-Gluc surface was detected. (e) Dot blot detection of biotinylated EVs. EVs isolated from HEK293T cells stably expressing sshBirA with either GlucB (top) or Gluc (bottom) were dot blotted on nitrocellulose membranes in a dose range followed by probing with streptavidin-HRP and chemiluminescence detection. EV-GlucB showed quantity-dependent biotinylated EVs, whereas EV-Gluc control exhibited no biotinylation background signal. (f) Nanoparticle tracking analysis (NTA) of EVs. Similar size distribution between EV-Gluc (peaks: 67, 100, and 177 nm) and EV-GlucB (81, 104, and 175 nm) vesicles was detected.

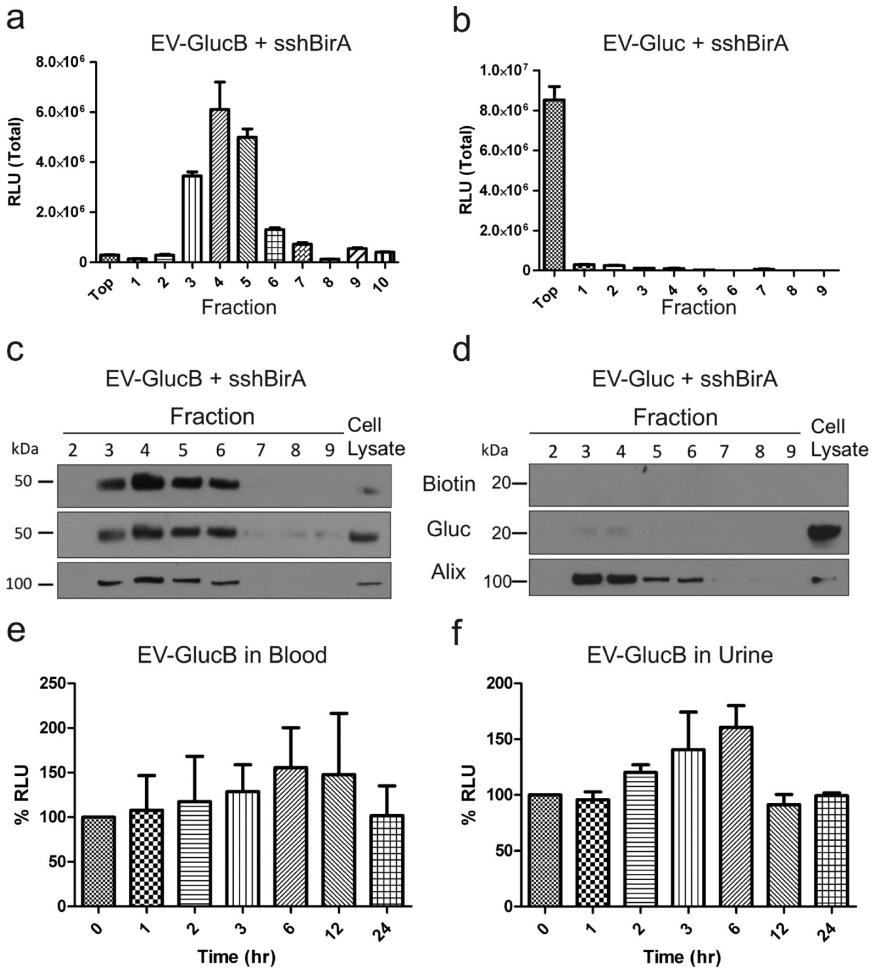

Figure 3. EV-GlucB exhibited EV-specific Gluc activity and was stable in blood and urine *ex vivo* over time. (a, b) Gluc activity assay of EV-GlucB (a) and EV-Gluc (b) vesicles following sucrose gradient fractionation. Note distinct increase in Gluc activity of EV-GlucB in EV-containing fractions (#3, 4, 5) when compared to EV-Gluc. (c, d) Western blot analysis of proteins extracted from pelleted fractions demonstrated significant Gluc expression and biotinylation of EV-GlucB (c), but not on EV-Gluc (d). Exosomal marker Alix (95 kDa) was immunoprobed to identify exosome-containing fractions. Cell lysates of HEK293T cells stably expressing sshBirA with GlucB and Gluc were used as positive controls. (e, f) Gluc activity of EV-GlucB was stable in biofluids *ex vivo* over 24 h. Blood (e) and urine (f) collected from untreated animals were spiked with EV-GlucB vesicles and incubated at 37 °C, and samples were collected at different time points over 24 h. No significant loss of EV-GlucB signal was detected in either type of biofluid. $p > 0.05$ by one-way analysis of variance (ANOVA) at all time points.

ribosome entry site (IRES) and (2) sshBirA-IRES-mCherry, a biotin ligase codon optimized for mammalian gene expression and present within the secretory pathway (Figures 1, 2a).[8,9,19] Western blot analysis of the cells confirmed GlucB and Gluc expression and showed sshBirA greatly enhances biotinylation of the GlucB reporter (Figure 2b). EVs were next evaluated by transmission electron microscopy, which demonstrated successful surface display of Gluc and biotin on EV-GlucB vesicles and not on EV-Gluc vesicles (Figure 2c,d). To further confirm that GlucB labels and yields functional biotinylation of EVs, isolated EVs were dot blotted on nitrocellulose membranes followed by probing with streptavidin-horseradish peroxidase (HRP), which demonstrated a quantity-dependent biotinylation of EV-GlucB and no biotinylation of EV-Gluc (Figure 2e). Nanoparticle tracking analysis (NTA) showed a similar size distribution pattern between EV-Gluc and EV-GlucB vesicles, indicating labeling of EVs with GlucB does not alter physical properties of EVs when compared to unlabeled EV-Gluc (control) (Figure 2f).

EV-GlucB Exhibited EV-Specific Gluc Activity and Stability in Biofluids *ex Vivo*. To examine whether EV-GlucB contained active luciferase, isolated EVs were subjected to sucrose gradient fractionation followed by Gluc activity assay. EV-GlucB exhibited a greater than 10^6-fold increase in Gluc activity when compared to EV-Gluc (control) in vesicle-containing fractions (Figure 3a; #3−6). Moreover, the majority of Gluc activity in EV-Gluc was detected in the top layer above the sucrose gradient, indicating that the naturally secreted Gluc is not incorporated into EVs and remains mostly as free protein (Figure 3b). Proteins collected from the pelleted fractions were further analyzed by Western blotting and showed specific EV labeling of both Gluc and biotin in fractions 3−6 of the EV-GlucB samples, coinciding with fractions

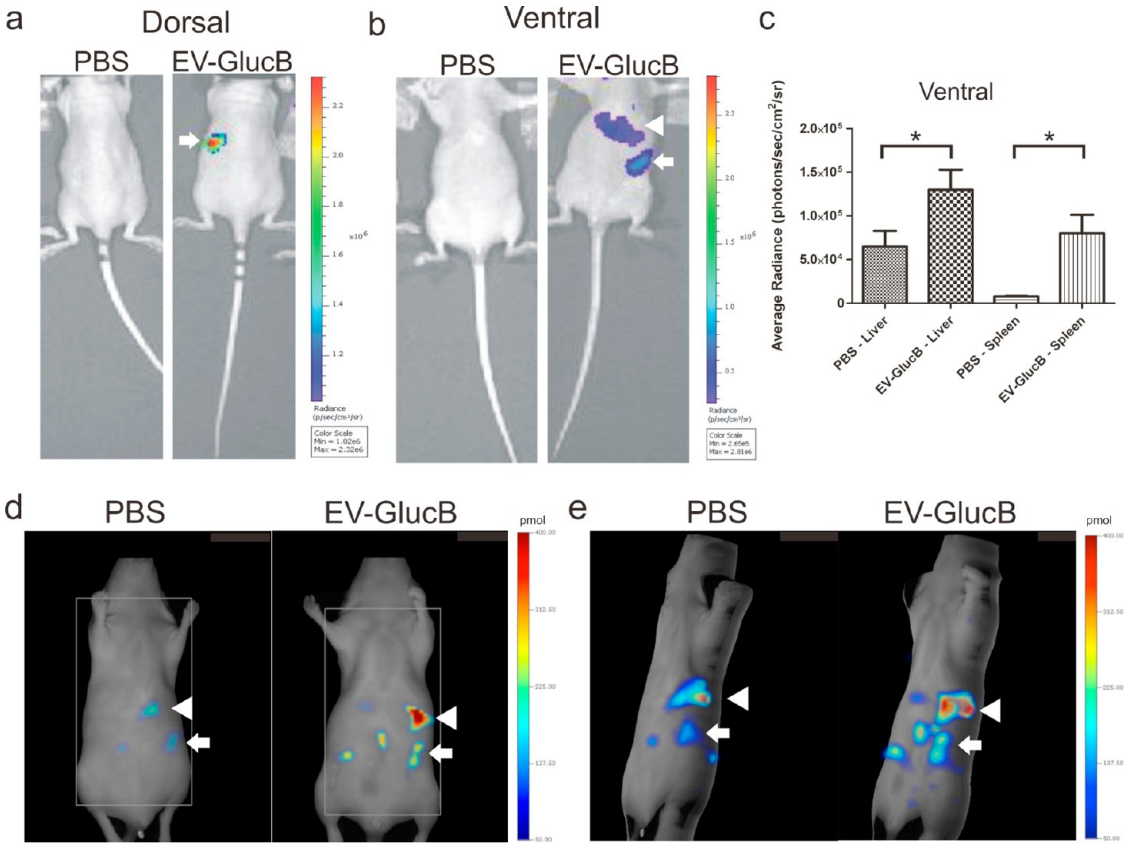

Figure 4. *In vivo* **imaging of iv-administered EVs. (a, b) Bioluminescence imaging of EV-GlucB in athymic nude mice. Animals were administered a bolus of either PBS (control) or EV-GlucB *via* the retro-orbital vein. CTZ was injected by the same route at 30 min postinitial administration to image EV-GlucB. (a) Representative image showing dorsal side of nude mouse with a prominent signal at regions corresponding to the spleen (arrow) in EV-GlucB-administered animals. (b) Imaging of ventral side showing a significant signal at regions corresponding to the spleen (arrow) and liver (arrowhead) in EV-GlucB-treated mice. No appreciable signal was detected on either side of PBS-injected mice. (c) Quantitation of EV-GlucB signal from bioluminescence imaging at ventral regions corresponding to the liver and spleen at 60 min post-EV administration. Sr, steradian. *$p < 0.05$ by Student's *t* test. (d, e) FMT imaging of EV-GlucB in athymic nude mice. Alexa680-conjugated EV-GlucB or PBS (control) was administered *via* the tail vein and imaged with FMT at 30 min postinjection. (d) Single Z plane of FMT imaging showing elevated fluorescence signal predominantly at the spleen (arrow) and the liver (arrowhead) in Alexa680-EV-GlucB, but not in control-treated mice. (e) 3D representation of FMT imaging illustrating Alexa680-EV-GlucB localizing mainly to the spleen (arrow) and the liver (arrowhead). A low level of background signal was also detected in the control.**

containing the exosomal marker, Alix (Figure 3c,d).[21] To test whether EV-GlucB is stable or may degrade rapidly in biofluids, blood and urine samples obtained from athymic nude mice spiked with EV-GlucB and incubated at 37 °C over 24 h showed no significant loss in Gluc activity (Figure 3e,f). Therefore, biofluid samples collected at different time points from the following *in vivo* experiments should reveal the level of EV-GlucB biofluids at the time of collection, but not necessarily the stability of EV-GlucB in circulation *in vivo*. These findings confirm EV-specificity of the EV-GlucB reporter, as well as stability of the luciferase activity in biofluids *ex vivo*.

Multimodal *in Vivo* Imaging of iv-Administered EV-GlucB. To visualize and track the distribution of intravenously administered EVs *in vivo*, EV-GlucB or phosphate-buffered saline (PBS; control) was injected into athymic nude mice *via* the retro-orbital vein. Thirty minutes post-EV treatment, CTZ injection revealed a significant amount of Gluc signal in the spleen and liver in EV-GlucB-injected mice, but not the controls (Figure 4a,b). This observation was confirmed by quantitation of average bioluminescent radiance from ventral side images, which showed a significantly higher signal in the liver and spleen of EV-GlucB-treated mice when compared to controls (Figure 4c).

To test the multimodality imaging capability of this EV reporter, EV-GlucB or PBS was labeled with streptavidin-Alexa680 conjugate followed by centrifugal filtration to remove unbound residues. The labeled EVs were then injected *via* the tail vein into athymic nude mice and imaged with FMT (30 min later), which revealed EV localization to the spleen and the liver similar to the distribution seen by Gluc bioluminescence imaging (Figure 4d,e).

Biodistribution of iv-Administered EV-GlucB. To confirm findings from *in vivo* EV imaging and further investigate tissue distribution of iv-injected EVs, organs were collected at different time points post-EV treatment to assess for Gluc activity. In agreement with results from *in vivo* imaging experiments, the highest EV signal was

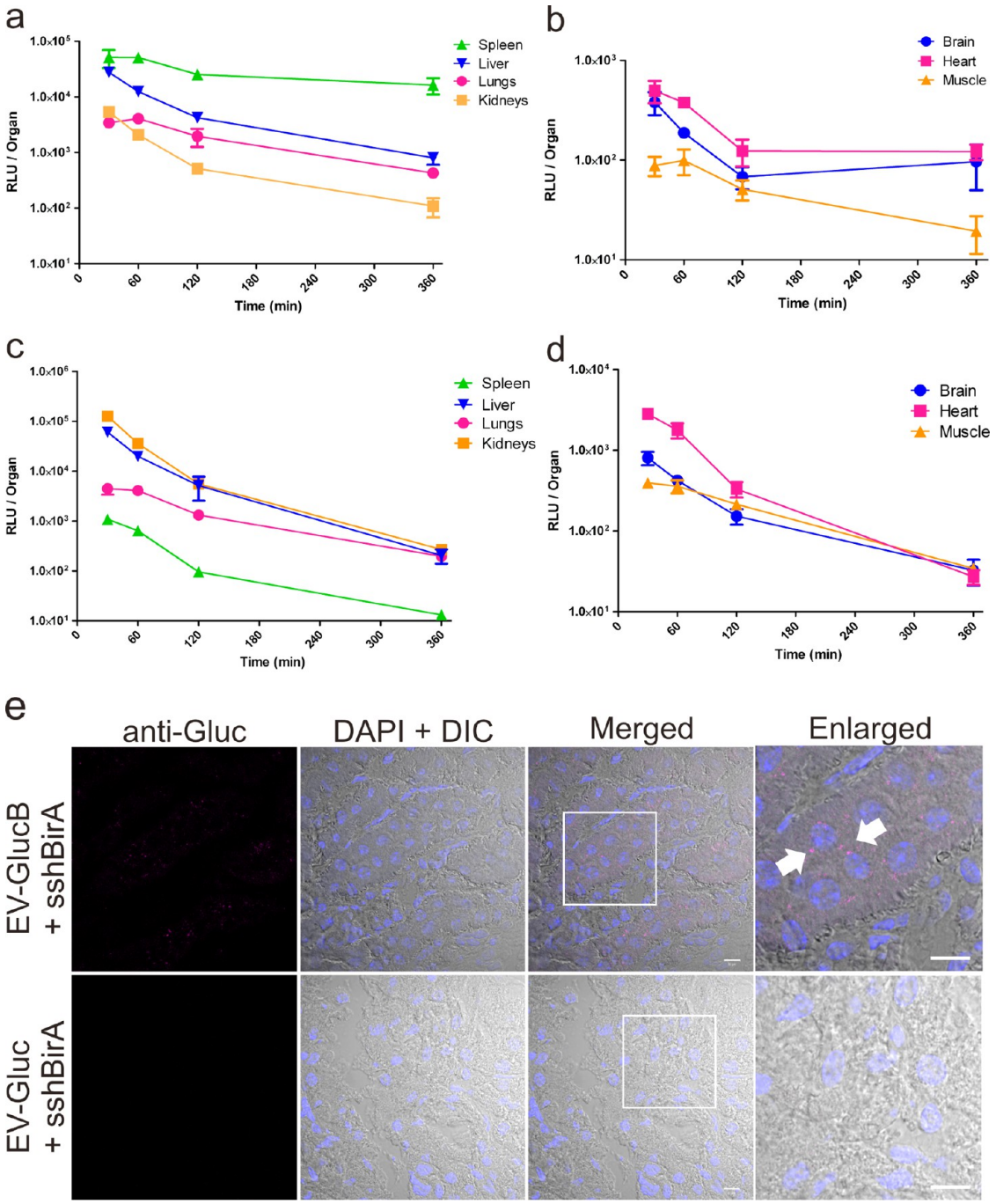

Figure 5. Biodistribution and retention of iv-administered EV-GlucB. (a, b) Biodistribution of iv-injected EV-GlucB *via* tail vein over time. Gluc activity was measured from organs collected from mice at different time points following EV-GlucB injection without transcardial perfusion with PBS. (c, d) Tissue retention of iv-injected EV-GlucB *via* tail vein over time in perfused tissues. Organs were collected from EV-injected animals at the same time points as above following transcardial perfusion with PBS. (e) Subcellular visualization of EV-GlucB in perfused kidneys by confocal microscopy. Kidney samples were collected from mice 30 min after iv-administration of EV-GlucB or EV-Gluc and transcardial perfusion with PBS, then cryosectioned and immunostained with anti-Gluc (rabbit) and Alexa Fluor 647 goat anti-rabbit antibodies. EV-GlucB (arrow) was detected in a punctate pattern in the perinuclear region of renal cells. EV-Gluc was used as a negative control for nonspecific binding or packaging of secreted Gluc protein in EVs and unspecific binding of the anti-Gluc antibodies to EVs. Nuclei were visualized by 4,6-diamidino-2-phenylindole (DAPI). DIC, differential interference contrast. Bar, 10 μm.

detected in the spleen followed by the liver, then the lungs and kidneys (Figure 5a). By comparison the brain, heart, and muscle showed lower amounts of signal across all time points (Figure 5b). All the above tissues were evaluated in their entirety, while a portion of skeletal muscle (hind leg) was sampled as an internal control to assess EV signal in nonorgan tissues. Notably, whereas EV signal decreased by more than half from 30 to 60 min in the liver and the kidneys (liver: 27 792 $\pm$ 4171 to 12 620 $\pm$ 2589 RLU; kidneys: 5448 $\pm$ 1102 to 2162 $\pm$ 192 RLU),

the spleen and the lung levels stayed relatively constant with no significant reduction in EV signal during this period (spleen: 51 227 ± 18 146 to 50 899 ± 8285 RLU; lungs: 3438 ± 335 to 4090 ± 821 RLU). At 360 min, the spleen and the heart had the most EV signal remaining as compared to the 30 min time point (spleen: 46.9 ± 22.4%; heart: 31.6 ± 9% of initial levels), whereas the lungs, the liver, and the kidneys showed the least (lung: 13.3 ± 2.4%; liver: 3.9 ± 1.3%; kidneys: 3.6 ± 0.6%). By contrast, the brain reached baseline signal at the 120 min time point (Supporting Information Figure 1), indicating minimal EV distribution to this organ. Interestingly, the muscle retained a significant fraction of activity (muscle: 45.1 ± 9%) out to 120 min.

Previous studies have used lipophilic dyes to label EVs to study their *in vivo* properties, as they, at least initially, provide a robust signal for EV detection.[8,13,14,17,22] However, these dyes, including PKH26 (red fluorescent dye) and PKH2 and PKH67 (green fluorescent dyes) are reported to have an *in vivo* half-life ranging from 5 to >100 days. Thus while the dyes may assist in "marking a trail" of where the administered EVs have been trafficked to *in vivo*, the persistence of the dye may outlast the labeled EVs *in vivo*. That is, dye-labeled EVs may be degraded and/or recycled *in vivo* while the dyes themselves remained intact and visible in the tissues over time, yielding inaccurate spatiotemporal information regarding the fate of the EVs *in vivo*. The reporter described here employs *Gaussia* luciferase (Gluc), which emits flash bioluminescence (480 nm peak) that is over 1000-fold more sensitive than commonly used *Renilla* and firefly luciferases.[23] Moreover, metabolic biotinylation of surface receptors using BAP and bacterial biotin ligase allows multimodal imaging *in vivo*, including magnetic resonance imaging (MRI), single-photon emission computed tomography/positron emission tomography (SPECT/PET), and FMT (this study).[18] Combining both Gluc and biotin, we created an EV-specific reporter with high sensitivity and multimodal imaging capacity to study *in vivo* dynamics of systemically administered EVs.

Biodistribution analysis of GlucB-labeled EVs also revealed a short half-life of less than 30 min *in vivo* in most tissues. Whereas most EV-GlucBs were cleared from the animals by 6 h postinjection, previous reports detected a significant amount of dye-labeled EVs in tissues out to 24 h.[8,22] Similar to studies with systemically delivered dye-labeled EVs at early time points,[8,22] we observed the highest EV-GlucB levels in the spleen followed by the liver, kidneys, and lungs. On the other hand, melanoma-derived EVs (approximately 5 μg; ≤50 nm in diameter) were found to localize mostly to the liver followed by the lungs, kidneys, and spleen.[24] The difference may be attributed to the cell type producing the EVs used, as well as a variation in EV isolation methods, both of which dictate the shape, size, surface protein, lipid composition, and population of purified EVs.[25,26] In addition, unprocessed dye following EV clearance and/or degradation may remain in tissues, resulting in inaccurate spatiotemporal resolution of EVs *in vivo*. Based on a previous study carried out with different sized liposomes,[27] it is inferred that ≤220 nm-sized EVs have an overall higher cargo encapsulation ratio than ≤50 nm-sized EVs, making ≤220 nm a model size range for EVs used here. While it is beyond the scope of the current study, it remains to be investigated whether EV donor cell type and preparation protocol affect subsequent biodistribution and clearance *in vivo*.

Retention of iv-Administered EV-GlucB in Organs. To elucidate organ uptake and retention of iv-administered EVs into tissues *per se* rather than into the combination of tissues and blood within them, EV-injected animals were transcardially perfused with PBS before collecting the organs/muscle at different time points. Surprisingly, perfused kidneys, and not the spleen, showed the highest EV signal followed by the liver, lung, heart, brain, and muscle (Figure 5c,d). Perfused spleen showed minimal EV-GlucB signal across all time points, suggesting EVs are not efficiently taken up into these cells despite the high amount of EVs present in blood passing through the highly vascularized spleen (Figure 5a,c). Perfused liver and lungs showed a similar trend in EV signal reduction from 30 to 60 min (liver: 60 783 ± 7565 to 20 118 ± 1666; lung: 4532 ± 1114 to 4148 ± 861 RLU) as compared to their nonperfused counterparts, indicating the EVs are actively taken up by these organs, likely for processing and degradation (Figure 5c). The brain, heart, and muscle also showed a comparable trend in EV signal reduction during this period (brain: 910 ± 152 to 529 ± 39; heart: 2849 ± 1814 to 1814 ± 376 RLU; muscle: 410 ± 40 to 50 ± 3 RLU), showing EV-GlucB are delivered and taken up by these organs, albeit in low amounts (Figure 5d).

To verify elevated EV-GlucB localization in the perfused kidneys, cryosections of the kidneys were immunolabeled with anti-Gluc antibodies, and a robust signal was detected only in EV-GlucB-injected and not EV-Gluc control samples (Figure 5e). Interestingly, most EV-GlucB staining was detected as punctate in the perinuclear region of the renal cells, similar to previous *in vitro* findings when recipient cells were treated with dye-labeled EVs.[5,8,28] However, we speculate the heightened EV retention in the perfused kidneys is an artifact of perfusion where EVs in the blood are forced into and trapped by the kidneys pending urination, resulting in greatly elevated EV retention in the perfused kidneys.

Very limited EV signals were detected in the brain and heart, indicating that only a small amount of EVs are delivered (possibly due to the blood−brain barrier for the brain) and/or taken up there.[13] Notably, since hind leg muscle samples (with an average weight of 87 mg per sample; approximately 1% of total skeletal muscle) consistently showed an appreciable level of EV-GlucB signal, and considering that skeletal muscles

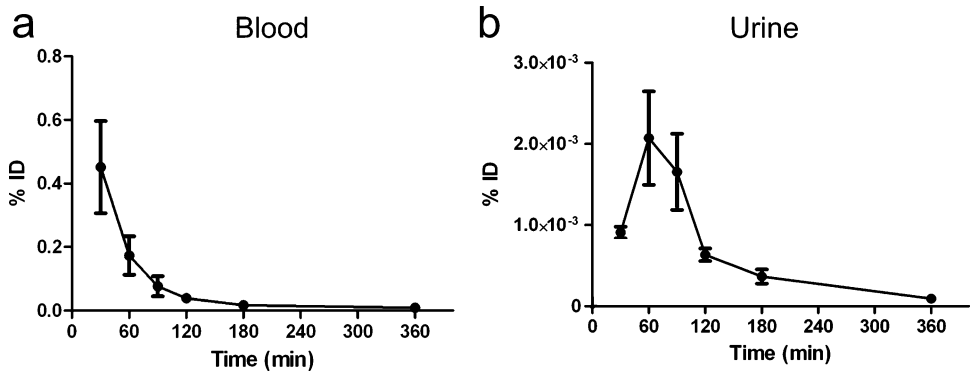

Figure 6. EV-GlucB distribution in biofluids. Blood (a) and urine (b) were collected at various time points after iv-injection of EV-GlucB, and Gluc activity was measured to evaluate blood levels and urine clearance of EV-GlucB. % ID, percent of initial dose.

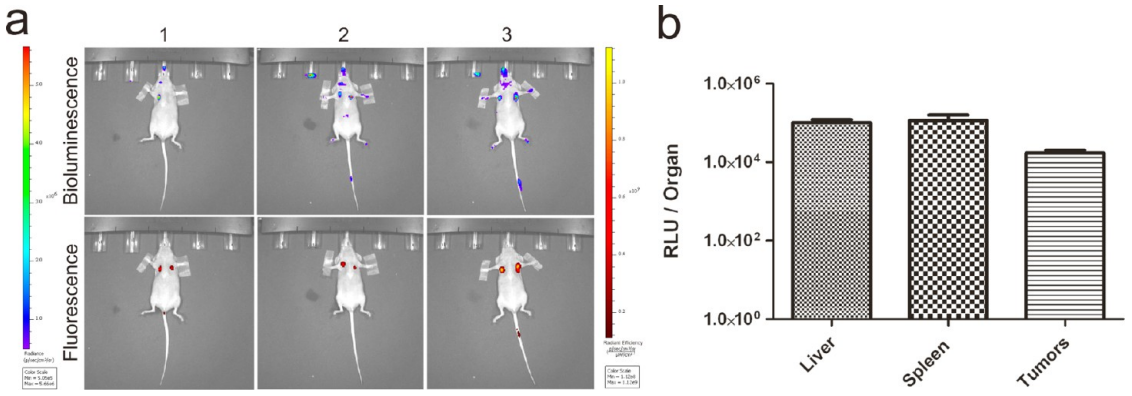

Figure 7. EV-GlucB localization to subcutaneous xenograft tumors. (a) Bioluminescence imaging for EV-GlucB administered iv (top row) into nude mice bearing subcutaneous xenograft tumors visualized by fluorescence imaging (bottom row; images shown for three mice). Stable Gli36 human glioma cells expressing mCherry (Gli36-mCherry) were implanted subcutaneously into left and right chest regions of athymic nude mice. Upon tumor development, animals were administered with a bolus of 100 μg of EV-GlucB *via* the tail vein, and CTZ was introduced *via* the retro-orbital vein at 60 min post-EV injection to track EV-GlucB by bioluminescence (left bar; photon/s/cm^2/sr). Tumor locations were verified by mCherry signal in radiant efficiency (right bar; [photon/s/cm^2/sr]/[μm/cm^2]) *via* fluorescence imaging. (b) Quantitation of EV-GlucB distribution in five tumor-bearing mice. Gluc activity was determined from the livers, spleen, and tumors collected at 60 min post-EV administration. $p < 0.09$ by one-way ANOVA with Tukey's *post hoc* test.

in a female mouse make up to 64% of body weight,[29] a significant portion of EV-GlucB may be delivered to the skeletal muscles *via* iv-administration.

The predominant EV localization in the nonperfused spleen may be attributed to (i) the applied EV dosage (100 μg), which may be an excess amount, resulting in saturation of liver macrophages, which bind and endocytose particles, resulting in higher "free" EV level in the blood and consequently "spillover" into the spleen vasculature,[27] and/or (ii) lymphocytes or macrophages, which bind or absorb the EVs in the blood and traffic to the spleen. In fact, transcardial perfusion revealed that the spleen tissue itself retained little EV signals, suggesting that it serves as a transitory reservoir under conditions of excess EVs. It remains to be determined if lower dosages of EVs would abolish this phenomenon with increasing levels in the liver relative to the spleen for clinical considerations. On the other hand, and if this interpretation is valid, it may be possible to utilize the high dosage as a means to prolong EV exposure to the spleen for therapeutic strategies and use it as a "storage depot" for subsequent delivery to other tissues.

Blood Level and Urine Clearance of iv-Administered EV-GlucB. To investigate the dynamics of exogenously administered EVs *in vivo*, blood and urine were collected over time from EV-GlucB-injected animals, and luciferase activity was measured (Figure 6a,b). The highest EV-GlucB signal was detected in the blood at the earliest time point measured, 30 min, followed by a rapid decrease at 60 min and then a gradual decrease from 90 to 360 min (Figure 6a). A two-phase exponential decay equation model revealed that EVs in the blood first undergo a distribution phase with a short half-life of 19.9 $\pm$ 7.7 min followed by an elimination phase with a longer half-life of 184.5 $\pm$ 7.4 min. By contrast, EV-GlucB signal in the urine peaked at 60 min followed by a rapid reduction from 60 to 120 min ((2.07 $\pm$ 0.58) $\times$ 10^{-3} to (0.63 $\pm$ 0.080 $\times$ 10^{-3} % ID) and then a gradual decrease from 120 to 360 min (0.09 $\pm$ 0.04 $\times$ 10^{-3} % ID) (Figure 6b). While levels of EV-GlucB

activity in the blood and organs were highest at 30 min followed by a steady reduction out to 360 min, the highest levels of EV-GlucB in urine occurred at 60 and 120 min, suggesting that a small amount of EV-derived GlucB is cleared *via* the renal route following the distribution phase and hepatic clearance. At 360 min, minimal signal was detected in the blood, while some organs (notably the spleen) and the urine still retained a small portion of signal, indicating a small proportion of EV-GlucB remains active in the organs and then is cleared *via* the kidneys.

These findings also support the heightened EV retention in the perfused kidneys probably as an artifact of perfusion, where EVs in the blood are forced into and trapped by the kidneys. This is shown by the significant reduction in EV-GlucB levels in the perfused kidneys from 30 to 60 min post-treatment, which coincides with the increasing levels of Gluc activity detected in the urine during the same time period, indicating a small but appreciable fraction of vesicular protein is removed *via* renal clearance.

Altogether, most EV-GlucB was cleared from the organs and biofluids by 360 min post-iv administration, indicating active cellular uptake and degradation of the EVs by different cell types. Since the liver and lung showed the highest retention, we hypothesis the EVs, similar to liposomes, are actively taken up by phagocytic cells such as Kupffer cells and alveolar macrophages in the liver and lung, respectively, with eventual lysosomal degradation.[30] Albeit in a lower amount, a significant level of the reporter signal was detected in the urine. Combined with the observation that the EV signal was greatly elevated in the kidneys following transcardial perfusion, showing the EVs do circulate to that organ, we speculate that a small portion of the iv-administered EVs may be internalized by the kidney cells, such as podocytes, and subjected to degradation for release into the urine. The detailed cellular mechanism for internalization and processing of circulating EVs *in vivo* in different organs remains to be examined and warrants future investigations.

Systemic Administered EV-GlucB Was Quickly Trafficked to Tumors. Since solid tumors are often densely vascularized due to aberrant angiogenesis,[31] we speculated that solid tumors, like highly vascularized spleen, may accumulate EVs following systemic administration. To examine this possibility, athymic nude mice with subcutaneous Gli36-mCherry human glioma xenograft tumors in the left and right chest regions were injected with EV-GlucB *via* the tail vein and showed a prevalent level of EV signals at the tumor sites at 60 min postadministration as revealed by bioluminescence imaging (Figure 7a). Upon quantitation of EV-GlucB signals in isolated liver, spleen, and tumors, the tumors showed a significant amount of Gluc signal (Figure 7b), suggesting iv-injected EV-GlucB can be actively delivered to these tumors *via* systemic administration.

CONCLUSIONS

In this study, we addressed the *in vivo* properties of iv-administered EVs with accurate spatial and temporal resolution. For this, one needs a reporter that enables the following functions: (i) specific labeling of EVs; (ii) a multimodal platform for noninvasive EV imaging *in vivo* to accommodate different imaging techniques; and (iii) a robust and stable reporter that can signal nanometer-sized EVs in the organs, blood, and urine over time. The biotinylated EV-GlucB system described here fulfilled these demands and enabled tracking and monitoring of EVs, thereby revealing dynamic processing of EVs through different organs and clearance from blood and urine over time.

As EVs are negatively charged with phospholipids on their outer surface,[32] our findings are in line with pharmacokinetic studies using negatively charged, radiolabeled liposomes that reported an association of iv-administered liposomes with the mononuclear phagocyte system, mainly in the liver and spleen.[27,33] Moreover, only liposomes with 160 and 460 nm diameters showed an elevated disposition to the spleen and a decline in the liver with increasing concentration following iv-administration when compared to that of 58 nm-sized liposomes,[27] inferring a comparable size and dose-dependent biodistribution of EV-GlucB. Different amounts of EVs ranging from 4 to 150 μg protein content have been administered in mouse models,[8,13,22,24] and 100 μg protein of EVs ($\leq$220 nm in diameter) per mouse was used here as an experimental dosage, making these studies comparable. Future studies on the potential correlation between EV size, dosage, and pharmacokinetic properties will provide additional insights into EV-mediated therapies.

Notably, since cellular uptake of EVs depends on specific surface lipids and ligand–receptor pairing,[34–36] human HEK293T-derived EVs used in this study may exhibit a distinct biodistribution profile from that of mouse cell-derived EVs in the current mouse model, and this warrants future investigation. Moreover, as vesicular proteins vary from one cell type to the other,[37] it would be of interest to employ the high sensitivity of the current method to compare *in vivo* properties of endogenously released EV from different cell types, including normal and disease-associated cells. Given that cancer cells are known to produce an abundant amount of EVs and can display oncoproteins such as EGFRvIII on their surface,[7,8] cancer-derived EVs will likely exhibit different circulation, biodistribution, and clearance properties from their normal counterparts, with additional changes associated with tumor progression and response to treatment.

We also found iv-administered EV-GlucB to be quickly trafficked to subcutaneously xenograft tumors at one hour post-EV injection *in vivo*. Given that most solid tumors, and even premalignant neoplastic cells, are known to induce angiogenesis and exhibit leaky

vasculature,[31] these findings suggest EVs may serve as an effective vehicle to deliver therapeutic genes/agents to sites of tumor neovascularization.

In conclusion, our studies revealed a dynamic distribution and clearance process of systemically administered EVs with accurate spatiotemporal resolution previously unachievable using dye-based methods. The labeling method developed will provide insights into the role of EVs in different fields, including cancer, and their use in clinical therapy.

METHODS

Cell Culture. HEK293T (American Type Culture Collection, Manassas, VA, USA) and Gli36 human glioma cells (Dr. Anthony Capanogni, UCLA, Los Angeles, CA, USA) were cultured in high-glucose Dulbecco's modified Eagle's medium (Corning Cellgro, Manassas, VA, USA) supplemented with 10% fetal bovine serum (FBS) (Sigma, St. Louis, MO, USA), 100 U/mL penicillin, and 100 μg/mL streptomycin (Invitrogen) in a humidified cell culture-grade incubator with 5% CO_2 at 37 °C. EV-depleted FBS was prepared by centrifuging FBS at 100000*g* at 4 °C for 16 h followed by supernatant collection and filtration through a 0.22 μm filter (Millipore, Billerica, MA, USA).

EV Production and Isolation. Stable HEK293T cells expressing Gluc or GlucB with sshBirA were generated by transducing cells with previously described lentivirus vectors, CSCW-Gluc-internal ribosome entry site (IRES)-GFP or CSCW-GlucB-IRES-GFP, followed by infection with CSCW-sshBirA-IRES-mCherry lentiviruses.[18,19] Stable expression in cells was confirmed by Western blot analysis and microscopic examination using an inverted epifluorescence microscope (TE 200-U, Nikon, Melville, NY, USA) coupled to a digital camera.

To isolate EVs, briefly, conditioned medium was collected from cells incubated with culture medium supplemented with 10% EV-depleted FBS for 48 h followed by sequential centrifugation of the supernatant at 300*g* for 10 min and 2000*g* for 10 min at 4 °C and filtration through a 0.22 μm filter (Millipore). The filtrate was then subjected to ultracentrifugation at 100000*g* for 90 min at 4 °C,[5] and the EV pellets were resuspended with double-0.22 μm-membrane-filtered PBS. EV protein concentration was determined by Bradford protein assay (Bio-Rad, Hercules, CA, USA).

Protein Isolation and Western Blot Analysis. Stable HEK293T cells expressing Gluc or GlucB with sshBirA were lysed in radioimmunoprecipitation assay (RIPA) buffer containing protease inhibitors (complete, Mini, Roche Diagnostics, Indianapolis, IN, USA), and DNA was sheared by sonication. Protein concentration was determined by Bradford protein assay (Bio-Rad). Twenty micrograms of total protein was boiled for 2 min in SDS sample buffer, resolved by 10% SDS-PAGE gel with molecular weight standards (Precision Plus Protein All Blue Standards, Bio-Rad), and transferred onto nitrocellulose membranes.[19,38] The membranes were blocked with 5% bovine serum albumin (BSA) fraction V (Invitrogen, Grand Island, NY, USA) and immunoblotted with streptavidin-HRP conjugate (Pierce, Rockford, IL, USA), anti-Gluc (rabbit; Nanolight, Pinetop, AZ), and anti-GAPDH antibodies (mouse; Calbiochem, San Diego, CA, USA). This was followed by binding of secondary antibodies conjugated to HRP (Molecular Probes, Eugene, OR, USA) and signal detection with an enhanced chemiluminescent substrate (Pierce).

Transmission Electron Microscopy. Isolated EVs were pelleted at 20000*g* for 30 min at 4 °C followed by fixation with 4% formaldehyde in PBS for 2 h. Fixed EVs were cryosectioned and immunolabeled with anti-Gluc (mouse; Nanolight) and anti-CD63 (mouse; BD Biosciences, San Jose, CA, USA) followed by rabbit anti-mouse conjugated with 5 nm protein A-gold secondary antibodies (University Medical Center, Utrecht, The Netherlands). To detect EV surface biotinylation, fixed EVs were resuspended and immunolabeled with antibiotin antibodies (rabbit, Rockland Immunochemicals, Gilbertsville, PA, USA) followed by 5 nm gold-labeled secondary antibodies (Sigma). Images were captured using Tecnai G^2 Spirit Bio TWIN transmission electron microscope.

Dot Blot Detection of Biotinylated EVs. Gluc- or GlucB-labeled EVs in PBS were spotted onto nitrocellulose membranes at 16, 31, 63, 125, 250, 500, and 1000 ng of protein followed by overnight incubation in 5% BSA fraction V (Invitrogen), immunoblotting with streptavidin-HRP conjugate (Pierce), and chemiluminescence detection of biotinylated EVs with SuperSignal West Pico chemiluminescent substrate kit (Pierce) on autoradiography films (Denville Scientific, Metuchen, NJ, USA).

Nanoparticle Tracking Analysis. Isolated EV-Gluc and EV-GlucB were diluted 1000-fold with double-0.22 μm-membrane-filtered PBS and subjected to an LM10 nanoparticle analyzer (NanoSight, Duxbury, MA, USA) to determine size distribution using NTA software version 2.2.

Sucrose Gradient Ultracentrifugation. Isolated EVs were layered onto a sucrose density gradient consisting of 8, 30, 45, and 60% layers in PBS and centrifuged at 232500*g* for 38 min at 4 °C.[39] The top layer and the subsequent 10 fractions were collected. Twenty microliters of the top layer and each fraction were sampled for Gluc activity assay. To collect EV-containing pellets, the fractions were diluted 1:10 in PBS and centrifuged at 100000*g* for 1 h at 4 °C. Pellets were then resuspended in 25 μL of PBS or RIPA with protease inhibitor (mini, Complete, Roche Diagnostics) for Gluc activity assay or Western blot analysis, respectively.

Gluc Activity Assays. Fractions collected following sucrose gradient ultracentrifugation of EVs were diluted 1:50 in PBS, and 20 μL of the mixture was plated in triplicates into a white 96-well luminometer plate. Gluc activity was measured by an MLX microtiter plate luminometer (Dynex Technologies, Chantilly, VA, USA) with automated injection of 50 μL of CTZ (8 ng/mL; Nanolight) followed by photon counts for 10 s for each sample. EV-GlucB activity in organs was similarly measured with 20 μL of organ lysates in triplicates. To monitor EV-GlucB activity in blood *in vivo*, blood was sampled over time by creating a small nick at the mouse tail, mixed with 25 mM EDTA, and plated in triplicates of 5 μL. Urine sampled over time was similarly plated in triplicates of 10 μL. Fifty microliters of CTZ (50 ng/mL; Nanolight) was used to detect EV-GlucB activity in blood and urine samples. To examine the stability of EV-GlucB in biofluids, 15 μL of blood and urine were sampled from untreated athymic nude mice, spiked with 0.5 μg of EV-GlucB, and incubated for 1−3, 6, 12, and 24 h at 37 °C before measuring EV-GlucB activity as described above.

***In Vivo* Bioluminescence and FMT Imaging of EVs.** All animals (6 weeks old) were handled under practices and operating procedures complying with the policies of the MGH Review Board. For *in vivo* EV bioluminescence, three athymic nude mice were injected with a bolus of 100 μg of EV-GlucB or PBS *via* retro-orbital vein. Thirty minutes post-EV injection, 75 μL of CTZ mixture from "Inject-A-Lume" kit (Nanolight) was injected *via* a different retro-orbital vein for bioluminescence imaging (at 1 min post-CTZ injection) using an IVIS Spectrum connected to an XGI-8 anesthesia system (PerkinElmer, Waltham, MA, USA).

To study EV-GlucB distribution in tumor-bearing mice, five athymic nude mice were subcutaneously implanted with Gli36 cells (4×10^6) stably expressing mCherry on the left and right chest regions under anesthesia by intraperitoneal (ip) injection of a mixture of ketamine (100 mg/kg) and xylazine (3 mg/kg). When tumors reached a size of 3−5 nm in diameter (as monitored by mCherry fluorescence imaging), a bolus of 100 μg of EV-GlucB was administered *via* the tail vein, followed by an injection of 75 μL of CTZ mixture *via* the retro-orbital vein at 60 min post-EV injection. Bioluminescence images were captured as described above, and fluorescence images of stable Gli36-mCherry tumors were acquired using the same system under 605 nm excitation and 660 nm emission filters.

For FMT imaging of EVs, EV-GlucB (800 μg) was first conjugated with Alexa Fluor 680-streptavidin (80 μg) in 5% BSA-

containing PBS for 30 min at 4 °C, and excess dye was removed using an Amicon Ultra-15 100K centrifugal filter device (Millipore). A 100 μg amount of Alexa Fluor 680-conjugated EV-GlucB or PBS was injected *via* tail vein, and FMT imaging was carried out at 30 min post-treatment with the FMT2500 system connected to an RC2+ integrated anesthesia system (PerkinElmer).

Biodistribution Analysis and Immunocytochemistry. Athymic nude mice were injected with 100 μg of EV-GlucB *via* the tail vein and euthanized with ip injection of ketamine (300 mg/kg) and xylazine (30 mg/kg) at 30, 60, 120, and 360 min post-treatment. Transcardial perfusion with PBS was performed as previously described.[40] Brain, heart, lungs, liver, kidneys, spleen, and hind leg muscle (average of 87 mg of latter) were harvested from three nonperfused and four PBS-perfused mice per time point and snap frozen in liquid nitrogen. Organs were then weighed and finely diced, and 100 mg of each organ was homogenized with M-PER lysis buffer supplemented with protease inhibitors (Thermo Scientific, Rockford, IL, USA) for Gluc activity analysis. The baseline Gluc signal of each organ was determined as described above with nonperfused and PBS-perfused mice at 30 min following iv-injection with PBS. Total RLU per organ was calculated as follows and adjusted to baseline signal: (RLU/20 μL) $\times$ (500 μL M-PER lysis buffer/100 mg of organ) $\times$ (average organ weight in mg).

To detect and visualize EV-GlucB in kidney tissues, organs were harvested from EV-injected animals at 30 min and snap frozen with optimal cutting temperature compound in liquid nitrogen. Embedded kidneys were cryosectioned (12 μm thick) and immunostained with anti-Gluc (rabbit; Nanolight) and Alexa Fluor 647 goat anti-rabbit antibodies. Samples were imaged with an LSM510 confocal microscope and a 63$\times$ Zeiss Plan-Apochromat oil, 1.4NA objective (Zeiss, Thornwood, NY, USA).

Conflict of Interest: The authors declare no competing financial interest.

Acknowledgment. This work was supported by grants from NIH/NCI CA141150, CA069246, U19CA179563, and Voices Against Brain Cancer (VABC) (X.O.B.). C.P.L was supported by the Canadian Institute of Health Research (CIHR). We would like to thank R. Amante for his suggestions and discussion, P. Waterman for his help with FMT imaging, G. Lewandroski and D. Morse for the production of lentiviruses (MGH Vector Core, Boston, MA, USA, supported by NIH/NINDS P30NS045776 [B.A.T., X.O.B.]), Ran C. for IVIS Spectrum imaging assistance (Martinos Center for Biomedical Imaging, Boston, MA), and T. Diefenbach for microscope assistance (Ragon Institute Microscopy Core, Boston, MA).

Supporting Information Available: Baseline Gluc signal of nonperfused and PBS-perfused organs. This material is available free of charge *via* the Internet at http://pubs.acs.org.

REFERENCES AND NOTES

1. Lai, C. P.; Breakefield, X. O. Role of Exosomes/Microvesicles in the Nervous System and Use in Emerging Therapies. *Front. Physiol.* **2012**, *3*, 228.
2. Raposo, G.; Stoorvogel, W. Extracellular Vesicles: Exosomes, Microvesicles, and Friends. *J. Cell Biol.* **2013**, *200*, 373–383.
3. Davis, D. M.; Sowinski, S. Membrane Nanotubes: Dynamic Long-Distance Connections between Animal Cells. *Nat. Rev. Mol. Cell Biol.* **2008**, *9*, 431–436.
4. Goodenough, D. A.; Paul, D. L. Gap Junctions. *Cold Spring Harbor Perspect. Biol.* **2009**, *1*, a002576.
5. Skog, J.; Würdinger, T.; van Rijn, S.; Meijer, D. H.; Gainche, L.; Curry, W. T.; Carter, B. S.; Krichevsky, A. M.; Breakefield, X. O. Glioblastoma Microvesicles Transport RNA and Proteins That Promote Tumour Growth and Provide Diagnostic Biomarkers. *Nat. Cell Biol.* **2008**, *10*, 1470–1476.
6. Ratajczak, J.; Miekus, K.; Kucia, M.; Zhang, J.; Reca, R.; Dvorak, P.; Ratajczak, M. Z. Embryonic Stem Cell-Derived Microvesicles Reprogram Hematopoietic Progenitors: Evidence for Horizontal Transfer of mRNA and Protein Delivery. *Leukemia* **2006**, *20*, 847–856.
7. Al-Nedawi, K.; Meehan, B.; Micallef, J.; Lhotak, V.; May, L.; Guha, A.; Rak, J. Intercellular Transfer of the Oncogenic Receptor EGFRvIII by Microvesicles Derived from Tumour Cells. *Nat. Cell Biol.* **2008**, *10*, 619–624.
8. Peinado, H.; Alečković, M.; Lavotshkin, S.; Matei, I.; Costa-Silva, B.; Moreno-Bueno, G.; Hergueta-Redondo, M.; Williams, C.; García-Santos, G.; Ghajar, C. M.; *et al*. Melanoma Exosomes Educate Bone Marrow Progenitor Cells toward a Pro-Metastatic Phenotype through MET. *Nat. Med.* **2012**, *18*, 883–891.
9. Hood, J. L.; San, R. S.; Wickline, S. A. Exosomes Released by Melanoma Cells Prepare Sentinel Lymph Nodes for Tumor Metastasis. *Cancer Res.* **2011**, *71*, 3792–3801.
10. EL Andaloussi, S.; Mäger, I.; Breakefield, X. O.; Wood, M. J. A. Extracellular Vesicles: Biology and Emerging Therapeutic Opportunities. *Nat. Rev. Drug Discovery* **2013**, *12*, 347–357.
11. Tan, A.; De La Peña, H.; Seifalian, A. M. The Application of Exosomes as a Nanoscale Cancer Vaccine. *Int. J. Nanomed.* **2010**, *5*, 889–900.
12. Mizrak, A.; Bolukbasi, M. F.; Ozdener, G. B.; Brenner, G. J.; Madlener, S.; Erkan, E. P.; Ströbel, T.; Breakefield, X. O.; Saydam, O. Genetically Engineered Microvesicles Carrying Suicide mRNA/Protein Inhibit Schwannoma Tumor Growth. *Mol. Ther.* **2012**, *21*, 101–108.
13. Alvarez-Erviti, L.; Seow, Y.; Yin, H.; Betts, C.; Lakhal, S.; Wood, M. J. A. Delivery of siRNA to the Mouse Brain by Systemic Injection of Targeted Exosomes. *Nat. Biotechnol.* **2011**, *29*, 341–345.
14. Zhuang, X.; Xiang, X.; Grizzle, W.; Sun, D.; Zhang, S.; Axtell, R. C.; Ju, S.; Mu, J.; Zhang, L.; Steinman, L.; *et al*. Treatment of Brain Inflammatory Diseases by Delivering Exosome Encapsulated Anti-Inflammatory Drugs From the Nasal Region to the Brain. *Mol. Ther.* **2011**, *19*, 1769–1779.
15. Malam, Y.; Loizidou, M.; Seifalian, A. M. Liposomes and Nanoparticles: Nanosized Vehicles for Drug Delivery in Cancer. *Trends Pharmacol. Sci.* **2009**, *30*, 592–599.
16. Sun, D.; Zhuang, X.; Xiang, X.; Liu, Y.; Zhang, S.; Liu, C.; Barnes, S.; Grizzle, W.; Miller, D.; Zhang, H.-G. A Novel Nanoparticle Drug Delivery System: the Anti-Inflammatory Activity of Curcumin Is Enhanced When Encapsulated in Exosomes. *Mol. Ther.* **2010**, *18*, 1606–1614.
17. Silva, A. K. A.; Kolosnjaj-Tabi, J.; Bonneau, S.; Marangon, I.; Boggetto, N.; Aubertin, K.; Clément, O.; Bureau, M. F.; Luciani, N.; Gazeau, F.; *et al*. Magnetic and Photoresponsive Theranosomes: Translating Cell-Released Vesicles Into Smart Nanovectors for Cancer Therapy. *ACS Nano* **2013**, *7*, 4954–4966.
18. Niers, J. M.; Chen, J. W.; Lewandrowski, G.; Kerami, M.; Garanger, E.; Wojtkiewicz, G.; Waterman, P.; Keliher, E.; Weissleder, R.; Tannous, B. A. Single Reporter for Targeted Multimodal *in Vivo* Imaging. *J. Am. Chem. Soc.* **2012**, *134*, 5149–5156.
19. Niers, J. M.; Chen, J. W.; Weissleder, R.; Tannous, B. A. Enhanced *in Vivo* Imaging of Metabolically Biotinylated Cell Surface Reporters. *Anal. Chem.* **2011**, *83*, 994–999.
20. Tannous, B. A.; Grimm, J.; Perry, K. F.; Chen, J. W.; Weissleder, R.; Breakefield, X. O. Metabolic Biotinylation of Cell Surface Receptors for *in Vivo* Imaging. *Nat. Meth.* **2006**, *3*, 391–396.
21. Lee, T. H.; D'Asti, E.; Magnus, N.; Al-Nedawi, K.; Meehan, B.; Rak, J. Microvesicles as Mediators of Intercellular Communication in Cancer--the Emerging Science of Cellular "Debris". *Semin. Immunopathol.* **2011**, *33*, 455–467.
22. Ohno, S.-I.; Takanashi, M.; Sudo, K.; Ueda, S.; Ishikawa, A.; Matsuyama, N.; Fujita, K.; Mizutani, T.; Ohgi, T.; Ochiya, T. Systemically Injected Exosomes Targeted to EGFR Deliver Antitumor microRNA to Breast Cancer Cells. *Mol. Ther.* **2013**, *21*, 185–191.
23. Badr, C. E.; Tannous, B. A. Bioluminescence Imaging: Progress and Applications. *Trends Biotechnol.* **2011**, *29*, 624–633.
24. Takahashi, Y.; Nishikawa, M.; Shinotsuka, H.; Matsui, Y.; Ohara, S.; Imai, T.; Takakura, Y. Visualization and *in Vivo* Tracking of the Exosomes of Murine Melanoma B16-BL6 Cells in Mice after Intravenous Injection. *J. Biotechnol.* **2013**, *165*, 77–84.

25. Tauro, B. J.; Greening, D. W.; Mathias, R. A.; Ji, H.; Mathivanan, S.; Scott, A. M.; Simpson, R. J. Comparison of Ultracentrifugation, Density Gradient Separation, and Immunoaffinity Capture Methods for Isolating Human Colon Cancer Cell Line LIM1863-Derived Exosomes. *Methods* **2012**, *56*, 293–304.
26. Chaput, N.; Théry, C. Exosomes: Immune Properties and Potential Clinical Implementations. *Semin. Immunopathol.* **2011**, *33*, 419–440.
27. Abra, R. M.; Hunt, C. A. Liposome Disposition *in Vivo*. *Biochim. Biophys. Acta, Lipids Lipid Metab.* **1981**, *666*, 493–503.
28. Tian, T.; Wang, Y.; Wang, H.; Zhu, Z.; Xiao, Z. Visualizing of the Cellular Uptake and Intracellular Trafficking of Exosomes by Live-Cell Microscopy. *J. Cell. Biochem.* **2010**, *111*, 488–496.
29. Griffin, G. E.; Goldspink, G. The Increase in Skeletal Muscle Mass in Male and Female Mice. *Anat. Rec.* **1973**, *177*, 465–469.
30. Ahsan, F. Targeting to Macrophages: Role of Physicochemical Properties of Particulate Carriers—Liposomes and Microspheres—on the Phagocytosis by Macrophages. *J. Controlled Release* **2002**, *79*, 29–40.
31. Hanahan, D.; Weinberg, R. A. Hallmarks of Cancer: The Next Generation. *Cell* **2011**, *144*, 646–674.
32. Zwaal, R. F. A.; Bevers, E. M.; Comfurius, P.; Rosing, J.; Tilly, R. H. J.; Verhallen, P. F. J. Loss of Membrane Phospholipid Asymmetry during Activation of Blood Platelets and Sickled Red Cells; Mechanisms and Physiological Significance. *Mol. Cell. Biochem.* **1989**, *91*, 23–31.
33. Colley, C. M.; Ryman, B. E. Liposomes as Carriers *in Vivo* for Methotrexate. *Biochem. Soc. Trans.* **1975**, *3*, 157–159.
34. Théry, C.; Ostrowski, M.; Segura, E. Membrane Vesicles as Conveyors of Immune Responses. *Nat. Rev. Immunol.* **2009**, *9*, 581–593.
35. Miyanishi, M.; Tada, K.; Koike, M.; Uchiyama, Y.; Kitamura, T.; Nagata, S. Identification of Tim4 as a Phosphatidylserine Receptor. *Nature* **2007**, *450*, 435–439.
36. Escrevente, C.; Keller, S.; Altevogt, P.; Costa, J. Interaction and Uptake of Exosomes by Ovarian Cancer Cells. *BMC Cancer* **2011**, *11*, 108.
37. Simpson, R. J.; Kalra, H.; Mathivanan, S. ExoCarta as a Resource for Exosomal Research. *J. Extracell. Vesicles* **2012**, *1*, 18374.
38. Lai, C. P. K.; Bechberger, J. F.; Thompson, R. J.; MacVicar, B. A.; Bruzzone, R.; Naus, C. C. Tumor-Suppressive Effects of Pannexin 1 in C6 Glioma Cells. *Cancer Res.* **2007**, *67*, 1545–1554.
39. Maguire, C. A.; Balaj, L.; Sivaraman, S.; Crommentuijn, M. H.; Ericsson, M.; Mincheva-Nilsson, L.; Baranov, V.; Gianni, D.; Tannous, B. A.; Sena-Esteves, M.; *et al*. Microvesicle-Associated AAV Vector as a Novel Gene Delivery System. *Mol. Ther.* **2012**, *20*, 960–971.
40. Gage, G. J.; Kipke, D. R.; Shain, W. Whole Animal Perfusion Fixation for Rodents. *J. Vis. Exp.* **2012**, *65*, e3564.